Journal of
Applied Crystallography

ISSN 0021-8898

Received 16 August 2006
Accepted 10 April 2007

X-ray fluorescence correlation spectroscopy – a tool to study element-specific dynamics

Olaf Leupold,[a]* Gerhard Grübel,[a] Stephan V. Roth,[a] Christian Schroer,[b] Wojciech Roseker,[a] Marcin Sikorski[a] and Aymeric Robert[c]

[a]Hasylab, DESY, Notkestrasse 85, D-22607 Hamburg, Germany, [b]Institut für Strukturphysik, TU Dresden, D-01062 Dresden, Germany, and [c]ESRF, BP 200, F-38043 Grenoble, France. Correspondence e-mail: olaf.leupold@desy.de

We have explored the feasibility of X-ray fluorescence correlation spectroscopy for studying the dynamics of colloidal particles in solution. We measured suspensions of Au nanoparticles from 5 to 150 nm diameter in water/glycerol mixtures of various compositions. Time-averaged sample properties were traced *via* small-angle X-ray scattering. The contrast of the measured time-correlation functions scales as expected with the particle concentration in the sample. The time constants for translational diffusion and sedimentation in water/glycerol mixtures follow only qualitatively the expected behaviour.

1. Introduction

Photon-correlation spectroscopy (PCS), probing fluctuations in the scattering intensity to study particle dynamics in fluids, is a well established technique in both the visible light (Berne & Pecora, 1976) and the hard X-ray regimes [see *e.g.* Grübel & Zontone (2004) and references therein]. In visible light PCS or X-ray PCS (XPCS) it is important to have a coherent beam illuminating the sample, and to record the temporal fluctuations in the speckle pattern that are directly related to the dynamics of the scattering particles. Another approach is to record the fluctuations in the fluorescence radiation, quite frequently used with visible light (Berne & Pecora, 1976), and recently also reported for X-rays (X-ray fluorescence correlation spectroscopy, XFCS) in a pilot experiment by Wang *et al.* (1998). XFCS does not require a coherent beam. Instead, the beam has to be strongly focused and the fluorescent intensity from a region around the focal point is probed. Time fluctuations in the fluorescent intensity reveal density fluctuations in the probe volume and thus the dynamics of the system. One of the interesting features of XFCS is the element sensitivity related to absorption edges, which can be selected by the tunability of synchrotron radiation. In this paper, we employed compound refractive lenses (CRLs) (Snigirev *et al.*, 1996; Lengeler *et al.*, 2002) in order to create a micrometre-sized focal spot for the XFCS experiment, carried out on a suspension of colloidal gold particles.

2. Experimental

In this experiment, we studied suspensions of colloidal Au nanoparticles with diameters ranging from 5 to 150 nm in water and water/glycerol mixtures. The viscosity of the solvent was adjusted by choosing the water/glycerol ratio and by controlling the temperature. The X-ray energy was 12 keV, which is just above the L_3 absorption edge of gold. The experiment was performed at the ID10C station (Troika beamline) at the ESRF. The experimental setup is sketched in Fig. 1. A pair of mirrors suppresses higher harmonics from two U27 undulators. The Si(111) channel-cut monochromator yields an energy resolution of $\approx 10^{-4}$ at 12 keV. For the XFCS measurements, the monochromatic beam was focused by an arrangement of 75 compound refractive lenses made out of beryllium (Snigirev *et al.*, 1996; Lengeler *et al.*, 2002) located 580 mm from the sample. The size of the focal spot was about 9 × 6 μm^2 (full width at half-maximum, horizontal × vertical). The fluorescence radiation was measured by an energy resolving detector (detector 2 in Fig. 1). We used a silicon drift diode (Ketek AXAS) with an active area of 10 mm^2 and a nominal energy resolution of about 150 eV at 6 keV. Samples were measured in glass capillaries of 1 mm diameter installed in an evacuated sample chamber, in order to reduce parasitic scattering from air and Ar fluorescence radiation. Fig. 2 shows a typical fluorescence spectrum from a suspension of gold nanoparticles (particle size 150 nm). The Au $L\alpha$ fluorescence at about 9.7 keV (shaded area in Fig. 2) is clearly resolved from the 12 keV peak of the incident radiation. Lines at 8.05 and 8.9 keV correspond to Cu fluorescence

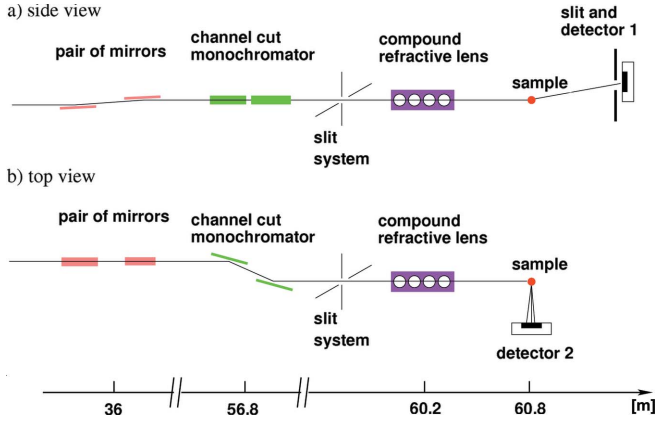

Figure 1
Experimental setup for XFCS and SAXS. (*a*) Side view of the setup for the SAXS measurement. A pair of vertically deflecting mirrors is followed by a horizontally deflecting Si(111) channel-cut monochromator. A slit system and a set of compound refracting lenses (CRLs) provides the micrometre-sized beam. Scattered photons are recorded by a fast avalanche photodiode (detector 1) at a distance of about 3 m, which performs Q scans in the vertical direction. Resolution in Q is provided by a 100 μm × 100 μm sized slit at the detector. (*b*) Top view of the setup for XFCS. The same optics are used as in (*a*). The energy-resolving silicon drift diode (detector 2) records fluorescence radiation in the horizontal plane.

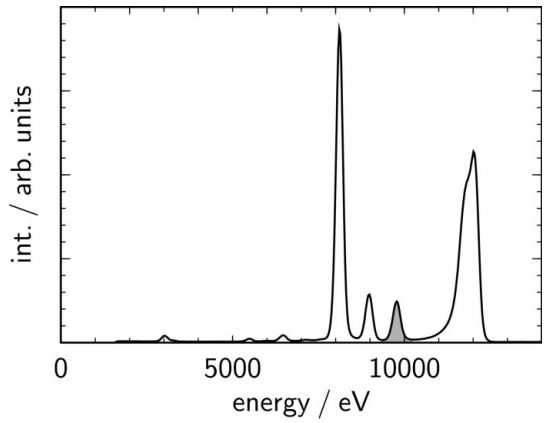

Figure 2
Energy spectrum of X-ray fluorescence from the sample. One can clearly resolve the 9.7 keV Au fluorescence (shaded area) from the 12 keV incident radiation and the Cu fluorescence from the sample holder at 8.05 and 8.9 keV.

from the sample-holder setup. For the XFCS measurements, the energy window of a single-channel analyzer (SCA) was carefully adjusted to the 9.7 keV fluorescence line. The SCA signal was used to record the intensity autocorrelation function of the Au fluorescence radiation employing a hardware correlator (Flex01D-08). There was a small background resulting from the low-energy shoulder of the 12 keV incident beam. For the small-angle X-ray scattering (SAXS) measurements, the Q dependence [$Q = 4\pi \sin(\theta)/\lambda$, with the X-ray wavelength λ and the scattering angle 2θ] of the scattering intensity was scanned with the help of an avalanche photodiode (APD) (detector 1 in Fig. 1) at a distance of about 2.3 m from the sample, with the Q resolution provided by the slit of 100 × 100 µm directly upstream of the APD.

3. Results

A typical SAXS pattern of a suspension of colloidal Au particles (with nominal diameter of 100 nm) is shown in Fig. 3. The fit to the data, shown as solid line in Fig. 3, is based on the equation

$$I(Q) \propto F(Q)S(Q), \qquad (1)$$

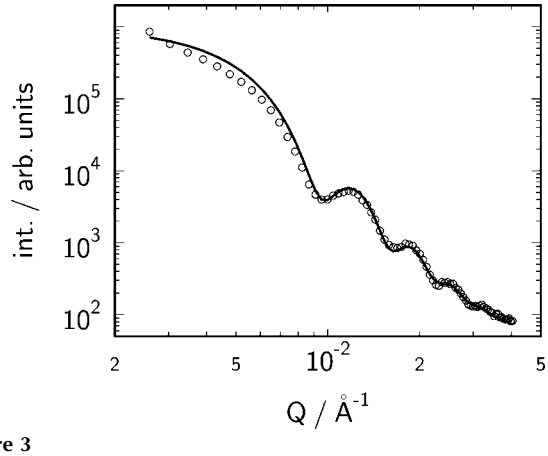

Figure 3
SAXS pattern (circles) and fit curve (solid line) for a 100 nm colloidal gold suspension, assuming spherical particles and including polydispersity and taking into account the Q resolution of the setup.

where the structure factor $S(Q) = 1$ due to the extremely high dilution of our samples. $F(Q)$ is the form factor for spherical particles and is given by

$$F(Q) \propto [3(\sin QR - QR\cos QR)/(Q^3R^3)]^2. \qquad (2)$$

The fit taking into account the Q resolution of the setup and a Schulz distribution (Schulz, 1939)

$$f(r, \langle r\rangle, z) = \frac{1}{z!}\left(\frac{z+1}{\langle r\rangle}\right)^{z+1} r^z \exp\left(-\frac{z+1}{\langle r\rangle}r\right) \qquad (3)$$

for the particle size r yields an average particle size $\langle r\rangle$ of 96 nm and a polydispersity $p = [1/(z+1)]^{1/2}$ of about 9%.

The XFCS data were taken on colloidal Au in several water/glycerol solvents. The fluorescent count rates reached up to 1 kHz in the selected energy window. Typical XFCS correlation functions are shown in Fig. 4 for gold particles of 150 nm diameter in a 1:10 water/glycerol mixture and in a 1:1 water/glycerol mixture at room temperature. The particle concentration was 1.7×10^9 particles per ml water for the 150 nm sized particles. The XFCS correlation function $g(t)$ is given by (Wang *et al.*, 1998):

$$g(t) = 1 + \langle N\rangle^{-1}(1 + t/\tau_d)^{-1} \exp\{-t^2/[\tau_s^2(1 + t/\tau_d)]\}, \qquad (4)$$

where $\langle N\rangle$ is the average number of particles in the scattering volume, which is determined by the concentration, the thickness of the capillary and the cross section of the focused beam, and τ_d and τ_s are the characteristic time constants for translational diffusive motion and sedimentation, respectively; they are both related to the beam sizes σ_x, σ_z (horizontal and vertical, respectively) *via* $\tau_d = \sigma_z\sigma_x/D_t$ and $\tau_s = \sigma_z/v$. Here, $D_t = k_BT/6\pi\eta R$ is the translational diffusion constant and $v = 2\Delta\rho gR^2/9\eta$ is the sedimentation velocity. R is the hydrodynamic radius of the particles, η is the viscosity of the solvent,

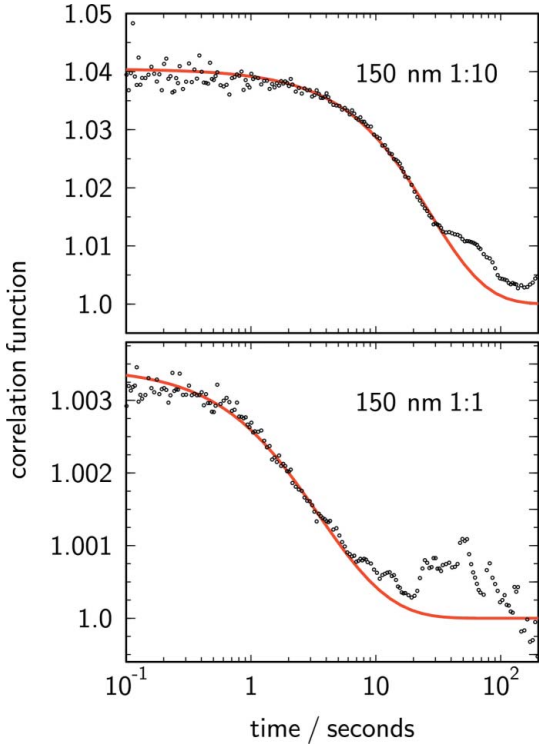

Figure 4
Measured time-correlation functions (circles) and fit curves (solid lines) for a 150 nm colloidal gold suspension with different water/glycerol ratios of the solvent.

Table 1
Average number of particles $\langle N \rangle$ and time constants for diffusion and sedimentation for two samples of colloidal gold in suspensions with different viscosities.

Ratio water/glycerol	$\langle N_{prep} \rangle$	$\langle N \rangle$	τ_d (s)	τ_s (s)
1:10	27	25	31	35
1:1	150	290	3.3	6.0

k_B is the Boltzmann constant, T is the sample temperature, $\Delta\rho$ is the density difference between Au and the solvent, and g is the gravitational acceleration. In the limit $t \rightarrow 0$

$$g(t \rightarrow 0) = 1 + \langle N \rangle^{-1}. \quad (5)$$

This explains that the amplitude of the correlation function is a measure of the particle density. An increase in contrast on dilution is observed in the correlation functions shown in Fig. 4. The amplitude in the diluted system (1:10) is 1.04, while for the 1:1 concentration one finds an amplitude of 1.0035. Both correlation functions decay to the base line, but with different time constants. This is expected, since both the characteristic time constants for translational diffusion and sedimentation are proportional to the viscosity of the solvent and thus depend on the glycerol content. In the 1:10 diluted sample, corresponding to a ten times larger glycerol content, one expects and observes much slower dynamics due to the larger viscosity compared with the 1:1 mixture. We have evaluated the measured correlation functions by applying equation (4). It turned out that both processes – translational diffusion and sedimentation – contribute to the decay of the correlation function.

The results of the fits are given in Table 1. The number of particles in the scattering volume as revealed from the fit using equation (4) (*i.e.* $\langle N \rangle$) is $\langle N \rangle = 25$ and $\langle N \rangle = 290$ for the two concentrations, 1:10 and 1:1, respectively. This is in fairly good agreement with the expected number $\langle N_{prep} \rangle$ obtained from the stoichiometry of the prepared samples. The time constants for translational diffusion and sedimentation obtained from the XFCS experiment can be compared with calculated values, based on the particle size revealed from the SAXS measurements and the estimated viscosity values for water/glycerol mixtures at room temperature. It turns out that our experimentally obtained time constants are significantly smaller than the expected values. The reasons for this discrepancy are not yet fully understood. One source of error is the viscosity of the water/glycerol solvent, which has not been determined experimentally but is based on extrapolated literature values.

4. Conclusions

For future experiments, a precise determination of the solvent viscosity and a smaller beam cross section at the sample are necessary, in order to resolve better both translational diffusion and sedimentation from the XFCS autocorrelation data.

References

Berne, B. J. & Pecora, R. (1976). *Dynamic Light Scattering*. New York: John Wiley and Sons.
Grübel, G. & Zontone, F. (2004). *J. Alloys Compds.* **362**, 3–11.
Lengeler, B., Schroer, C. G., Benner, B., Gerhardus, A., Günzler, T. F., Kuhlmann, M., Meyer, J. & Zimprich, C. (2002). *J. Synchrotron Rad.* **9**, 119–124.
Schulz, G. V. (1939). *Z. Phys. Chem. B*, **43**, 25–46.
Snigirev, A., Kohn, V., Snigireva, I. & Lengeler, B. (1996). *Nature (London)*, **384**, 49–51.
Wang, J., Sood, A. K. S., Satyam, P. V., Feng, Y., Wu, X., Cai, Z., Yun, W. & Sinha, S. K. (1998). *Phys. Rev. Lett.* **80**, 1110–1113.